

Subdiffraction incoherent optical imaging via spatial-mode demultiplexing

Mankei Tsang^{1,2,*}

¹*Department of Electrical and Computer Engineering,
National University of Singapore, 4 Engineering Drive 3, Singapore 117583*

²*Department of Physics, National University of Singapore, 2 Science Drive 3, Singapore 117551*

(Dated: March 4, 2022)

I propose a spatial-mode demultiplexing (SPADE) measurement scheme for the far-field imaging of arbitrary incoherent optical sources. For any object too small to be resolved by direct imaging under the diffraction limit, I show that SPADE can estimate the moments of the source distribution much more precisely than direct imaging can fundamentally do under the effect of photon shot noise.

I. INTRODUCTION

Recent research, initiated by our group [1–7], has shown that far-field linear optical methods can significantly improve the localization of two equally bright incoherent optical point sources when Rayleigh’s criterion is violated [8–14], overcoming previously established limits [15–18]. An open problem, of fundamental interest in optics and monumental importance to astronomy and fluorescence microscopy, is whether these results can be generalized for arbitrary incoherent sources. Here I take the first step towards solving the problem by proposing a generalized spatial-mode demultiplexing (SPADE) scheme for the imaging of incoherent source distributions. The use of coherent optical processing to improve the lateral resolution of incoherent imaging has thus far received relatively little attention, as prior proposals either have not demonstrated any substantial improvement or have not considered the important effect of noise [11, 19–22], while conventional wisdom suggests that any improvement should be modest [23]. Using quantum optics and parameter estimation theory, here I show that, for any object too small to be resolved by diffraction-limited direct imaging, SPADE can estimate the moments of the source distribution much more precisely than direct imaging can fundamentally do in the presence of photon shot noise. Given the importance of moments to imaging in identifying the size and shape of an object [24], the proposed scheme should provide a major boost to incoherent imaging applications that are currently limited by diffraction and shot noise [25–30].

II. QUANTUM OPTICS

To ensure rigor, I start with the quantum formalism established in Ref. [1]. The quantum state of incoherent light in M temporal modes can be written as $\rho^{\otimes M}$, where ρ can be expressed as

$$\rho = (1 - \epsilon)\rho_0 + \epsilon\rho_1 + O(\epsilon^2), \quad (2.1)$$

ϵ is the average photon number per mode assumed to be $\ll 1$ [29, 31], $\rho_0 = |\text{vac}\rangle\langle\text{vac}|$ is the vacuum state, ρ_1 is the one-photon state with its density matrix determined by the mutual

coherence function, and $O(\epsilon^2)$ denotes second-order terms, which are neglected hereafter. It is standard to assume that the fields from incoherent objects, such as stellar or fluorescent emitters, are spatially uncorrelated at the source [31]. In a diffraction-limited imaging system, the fields then propagate as waves; the Van Cittert-Zernike theorem is the most venerable consequence [31]. At the image plane of a conventional two-dimensional imaging system in the paraxial regime, this implies

$$\rho_1 = \int d^2\mathbf{R}\Lambda(\mathbf{R})|\psi_{\mathbf{R}}\rangle\langle\psi_{\mathbf{R}}|, \quad (2.2)$$

$$|\psi_{\mathbf{R}}\rangle = \int d^2\mathbf{r}\psi(\mathbf{r} - \mathbf{R})|\mathbf{r}\rangle, \quad (2.3)$$

where $\mathbf{R} = (X, Y)$ is the object-plane position vector, $\Lambda(\mathbf{R})$ is the source intensity distribution with normalization $\int d^2\mathbf{R}\Lambda(\mathbf{R}) = 1$, and $|\mathbf{r}\rangle = a^\dagger(\mathbf{r})|\text{vac}\rangle$ is a one-photon position eigenket on the image plane at position $\mathbf{r} = (x, y)$ with $[a(\mathbf{r}), a^\dagger(\mathbf{r}')] = \delta^2(\mathbf{r} - \mathbf{r}')$ [32], and $\psi(\mathbf{r})$ is the field point-spread function (PSF) of the imaging system. Without loss of generality, the image-plane position vector \mathbf{r} has been scaled with respect to the magnification to follow the same scale as \mathbf{R} [33]. For convenience, I also normalize the position vectors with respect to the width of the PSF to make them dimensionless.

Consider the processing and measurement of the image-plane field by linear optics and photon counting. The counting distribution for each ρ can be expressed as $\langle n_0, n_1, \dots | \rho | n_0, n_1, \dots \rangle$, where $|n_0, n_1, \dots\rangle = (\prod_{j=0}^{\infty} b_j^{\dagger n_j} / \sqrt{n_j!}) |\text{vac}\rangle$, $b_j \equiv \int d^2\mathbf{r}\phi_j^*(\mathbf{r})a(\mathbf{r})$, $\phi_j(\mathbf{r})$ is the optical mode function that is projected to the j th output, and $[b_j, b_k^\dagger] = \int d^2\mathbf{r}\phi_j^*(\mathbf{r})\phi_k(\mathbf{r}) = \delta_{jk}$. With the negligence of multiphoton coincidences, the relevant projections are $\{|\text{vac}\rangle, |\phi_j\rangle\}$, with $|\phi_j\rangle \equiv |0, \dots, n_j = 1, \dots, 0\rangle = b_j^\dagger |\text{vac}\rangle = \int d^2\mathbf{r}\phi_j(\mathbf{r})|\mathbf{r}\rangle$. The zero-photon probability becomes $1 - \epsilon$ and the probability of one photon being detected in the j th mode becomes $\epsilon p(j)$, where

$$p(j) \equiv \langle \phi_j | \rho_1 | \phi_j \rangle = \int d^2\mathbf{R}\Lambda(\mathbf{R})|\langle \phi_j | \psi_{\mathbf{R}} \rangle|^2 \quad (2.4)$$

is the one-photon distribution. For example, direct imaging can be idealized as a measurement of the position of each pho-

* mankei@nus.edu.sg

ton, leading to an image given by

$$\lambda(\mathbf{r}) \equiv \langle \mathbf{r} | \rho_1 | \mathbf{r} \rangle = \int d^2 \mathbf{R} \Lambda(\mathbf{R}) |\psi(\mathbf{r} - \mathbf{R})|^2, \quad (2.5)$$

which is a basic result in statistical optics [31, 33]. While Eq. (2.5) suggests that, similar to the coherent-imaging formalism, the PSF acts as a low-pass filter in the spatial frequency domain [33], the effect of more general optical processing according to Eq. (2.4) is more subtle and offers surprising advantages, as demonstrated by recent work [1–14] and elaborated in this paper.

Over M temporal modes, the probability distribution of photon numbers $m = (m_0, m_1, \dots)$ detected in the respective optical modes becomes

$$P(m) = \sum_L \mathcal{M}(m|L) \mathcal{B}(L), \quad (2.6)$$

where $\mathcal{B}(L)$ is the binomial distribution for detecting L photons over M trials with single-trial success probability ϵ and $\mathcal{M}(m|L) = \delta_{L, \sum_j m_j} L! \prod_j [p(j)]^{m_j} / m_j!$ is the multinomial distribution of m given L total photons [34]. Taking the limit of $\epsilon \rightarrow 0$ while holding $N = M\epsilon$ constant, $\mathcal{B}(L)$ becomes Poisson with mean N , and $P(m) \rightarrow \exp(-N) \prod_j [Np(j)]^{m_j} / m_j!$, which is the standard Poisson model of photon counting for incoherent sources at optical frequencies [5, 17, 25–31].

III. PARAMETER ESTIMATION

The central goal of imaging is to infer unknown properties of the source distribution $\Lambda(\mathbf{R})$ from the measurement outcome m . Here I frame it as a parameter estimation problem, defining $\theta = (\theta_1, \theta_2, \dots)$ as a vector of unknown parameters and assuming the source distribution $\Lambda(\mathbf{R}|\theta)$ to be a function of θ . Denote an estimator as $\hat{\theta}(m)$ and its error covariance matrix as $\Sigma_{\mu\nu}(\theta) = \sum_m P(m|\theta) [\hat{\theta}_\mu(m) - \theta_\mu][\hat{\theta}_\nu(m) - \theta_\nu]$. For any unbiased estimator ($\sum_m \hat{\theta}(m) P(m|\theta) = \theta$), the Cramér-Rao bound is given by [34]

$$\Sigma_{\mu\mu}(\theta) \geq \text{CRB}_{\mu\mu}(\theta), \quad \text{CRB}(\theta) \equiv J^{-1}(\theta), \quad (3.1)$$

where $J(\theta)$ is the Fisher information matrix given by

$$J_{\mu\nu}(\theta) \equiv \sum_m \frac{1}{P(m|\theta)} \frac{\partial P(m|\theta)}{\partial \theta_\mu} \frac{\partial P(m|\theta)}{\partial \theta_\nu}. \quad (3.2)$$

The bound is asymptotically attainable using the maximum-likelihood estimator for large N [34]. The Fisher information is regarded as the standard precision measure in modern incoherent imaging research [29, 35, 36], especially in fluorescence microscopy [17, 26–28].

To compute the information for Eq. (2.6), note that, for a given outcome m , the likelihood function is

$$P(m|\theta) = \mathcal{M}(m|L, \theta) \mathcal{B}(L|\theta), \quad L = \sum_j m_j, \quad (3.3)$$

and if ϵ is given so that \mathcal{B} does not depend on θ , the score functions with respect to P and \mathcal{M} are identical, viz., $\partial \ln P(m|\theta) / \partial \theta_\mu = \partial \ln \mathcal{M}(m|L, \theta) / \partial \theta_\mu$. This means that the Fisher information, which is also given by the covariance of the score function [34], can be obtained by computing the information for $\mathcal{M}(m|L, \theta)$ and then averaging it over $\mathcal{B}(L)$. This leads to

$$J_{\mu\nu}(\theta) = N \sum_j \frac{1}{p(j|\theta)} \frac{\partial p(j|\theta)}{\partial \theta_\mu} \frac{\partial p(j|\theta)}{\partial \theta_\nu}. \quad (3.4)$$

The Poisson model, being a limit of Eq. (2.6), naturally has the same expression for its information [15–17, 26, 28, 29]. For example, the direct-imaging information, given Eq. (2.5), is

$$J_{\mu\nu}^{(\text{direct})}(\theta) = N \int d^2 \mathbf{r} \frac{1}{\lambda(\mathbf{r}|\theta)} \frac{\partial \lambda(\mathbf{r}|\theta)}{\partial \theta_\mu} \frac{\partial \lambda(\mathbf{r}|\theta)}{\partial \theta_\nu}. \quad (3.5)$$

The effect of finite-size pixels can be similarly studied by assuming $p(j|\theta) = \int_{\mathcal{A}_j} d^2 \mathbf{r} \lambda(\mathbf{r}|\theta)$, where \mathcal{A}_j is the domain of each pixel, although the resulting information must be lower than Eq. (3.5) owing to a data-processing inequality [37].

IV. SPATIAL-MODE DEMULTIPLEXING (SPADE)

SPADE is a technique previously proposed for the purpose of estimating the separation between two incoherent point sources [1, 2, 9, 11–13]. I now ask how SPADE can be generalized for the imaging of an arbitrary source distribution. Consider the transverse-electromagnetic (TEM) basis $\{|\mathbf{q}\rangle; \mathbf{q} = (q_x, q_y) \in \mathbb{N}^2\}$ [38], where

$$|\mathbf{q}\rangle = \int d^2 \mathbf{r} \phi_{\mathbf{q}}(\mathbf{r}) |\mathbf{r}\rangle, \quad (4.1)$$

$$\phi_{\mathbf{q}}(\mathbf{r}) \equiv \frac{\text{He}_{q_x}(x) \text{He}_{q_y}(y)}{\sqrt{2\pi q_x! q_y!}} \exp\left(-\frac{x^2 + y^2}{4}\right), \quad (4.2)$$

and He_q is the Hermite polynomial [39, 40]. Assuming a Gaussian PSF given by $\psi(\mathbf{r}) = \phi_{00}(\mathbf{r})$, which is a common assumption in fluorescence microscopy [26, 28], $|\psi_{\mathbf{R}}\rangle$ is a coherent state [41], and the one-photon density matrix in the TEM basis becomes

$$g(\mathbf{q}, \mathbf{q}'|\theta) \equiv \langle \mathbf{q} | \rho_1(\theta) | \mathbf{q}' \rangle \quad (4.3)$$

$$= C(\mathbf{q}, \mathbf{q}') \int d^2 \mathbf{R} \Lambda(\mathbf{R}|\theta) e^{-(X^2 + Y^2)/4} \times X^{q_x + q'_x} Y^{q_y + q'_y}. \quad (4.4)$$

$$C(\mathbf{q}, \mathbf{q}') \equiv \frac{1}{2^{|\mathbf{q} + \mathbf{q}'|_1} \sqrt{\mathbf{q}! \mathbf{q}'!}}, \quad (4.5)$$

where I have introduced the shorthands

$$|\mathbf{q}|_1 \equiv q_x + q_y, \quad \mathbf{q}! \equiv q_x! q_y!. \quad (4.6)$$

To investigate the precision arising from SPADE measurements, define the parameters of interest as

$$\theta_\mu = \int d^2 \mathbf{R} \Lambda(\mathbf{R}|\theta) e^{-(X^2 + Y^2)/4} X^{\mu_x} Y^{\mu_y}, \quad (4.7)$$

with $\boldsymbol{\mu} = (\mu_X, \mu_Y)$, leading to a linear parameterization of g given by

$$g(\mathbf{q}, \mathbf{q}'|\theta) = C(\mathbf{q}, \mathbf{q}')\theta_{\mathbf{q}+\mathbf{q}'}. \quad (4.8)$$

Notice that each $\theta_{\boldsymbol{\mu}}$ is a moment of the source distribution filtered by a Gaussian. In particular, if the object is much smaller than the PSF width, the Gaussian can be neglected, and $\theta_{\boldsymbol{\mu}}$ becomes a moment of the source distribution itself. This subdiffraction regime is of central interest to superresolution imaging and, as shown in Sec. V, also a regime in which direct imaging performs relatively poorly. Since a distribution is uniquely determined by its moments [24], $\Lambda(\mathbf{R}|\theta) \exp[-(X^2 + Y^2)/4]$ and therefore $\Lambda(\mathbf{R}|\theta)$ can in principle be reconstructed given the moments. Note also that the object-moment order $\boldsymbol{\mu}$ is nontrivially related to the order of the matrix element via $\boldsymbol{\mu} = \mathbf{q} + \mathbf{q}'$, which is a peculiar feature of incoherent imaging.

A measurement in the TEM basis yields

$$p^{(\text{TEM})}(\mathbf{q}|\theta) = C(\mathbf{q}, \mathbf{q})\theta_{2\mathbf{q}}, \quad (4.9)$$

which is sensitive only to moments with even μ_X and μ_Y , as also recognized by Ref. [11]. The Cramér-Rao bound becomes

$$\text{CRB}_{\boldsymbol{\mu}\boldsymbol{\mu}}^{(\text{TEM})}(\theta) = \frac{\theta_{\boldsymbol{\mu}}}{NC(\boldsymbol{\mu}/2, \boldsymbol{\mu}/2)} \text{ for even } \mu_X \text{ and } \mu_Y. \quad (4.10)$$

To access the other moments, consider interferometry between two TEM modes that implements the projections

$$|+\rangle \equiv \frac{1}{\sqrt{2}}(|\mathbf{q}\rangle + |\mathbf{q}'\rangle), \quad |-\rangle \equiv \frac{1}{\sqrt{2}}(|\mathbf{q}\rangle - |\mathbf{q}'\rangle). \quad (4.11)$$

This two-channel interferometric TEM (iTEM) measurement leads to

$$\begin{aligned} p^{(\mathbf{q}, \mathbf{q}')}(|+\rangle|\theta) &= \beta(\mathbf{q}, \mathbf{q}') + C(\mathbf{q}, \mathbf{q}')\theta_{\mathbf{q}+\mathbf{q}'}, \\ p^{(\mathbf{q}, \mathbf{q}')}(|-\rangle|\theta) &= \beta(\mathbf{q}, \mathbf{q}') - C(\mathbf{q}, \mathbf{q}')\theta_{\mathbf{q}+\mathbf{q}'}, \end{aligned} \quad (4.12)$$

$$\beta(\mathbf{q}, \mathbf{q}') \equiv \frac{1}{2}[C(\mathbf{q}, \mathbf{q})\theta_{2\mathbf{q}} + C(\mathbf{q}', \mathbf{q}')\theta_{2\mathbf{q}'}]. \quad (4.13)$$

The dependence on $\theta_{\mathbf{q}+\mathbf{q}'}$ is the main interest here, as it allows one to access any moment parameter, but the probabilities also depend on a background parameter β . If β is unknown, the bound for $\theta_{\mathbf{q}+\mathbf{q}'}$ can be computed by taking the inverse of the two-by-two information matrix with respect to $(\beta, \theta_{\mathbf{q}+\mathbf{q}'})$. The result is

$$\text{CRB}_{\boldsymbol{\mu}\boldsymbol{\mu}}^{(\mathbf{q}, \mathbf{q}')}(\theta) = \frac{\beta(\mathbf{q}, \mathbf{q}')}{2NC^2(\mathbf{q}, \mathbf{q}')}, \quad \boldsymbol{\mu} = \mathbf{q} + \mathbf{q}'. \quad (4.14)$$

For multiparameter estimation and general imaging, multiple TEM and iTEM measurements are needed. To be specific, Table I lists a set of schemes that together can be used to estimate all the moment parameters, while Fig. 1 shows a graphical representation of the schemes in the (q_x, q_y) space. The use of neighboring modes in the proposed iTEM schemes is

motivated by the fact that the $C(\mathbf{q}, \boldsymbol{\mu} - \mathbf{q})$ factor in Eq. (4.14) is maximized if \mathbf{q} is as close to $\boldsymbol{\mu} - \mathbf{q}$ as possible. The bases in different schemes are incompatible with one another, so the photons have to be rationed among the schemes, by applying them sequentially through reprogrammable interferometers or spatial-light modulators [13, 42–44] for example.

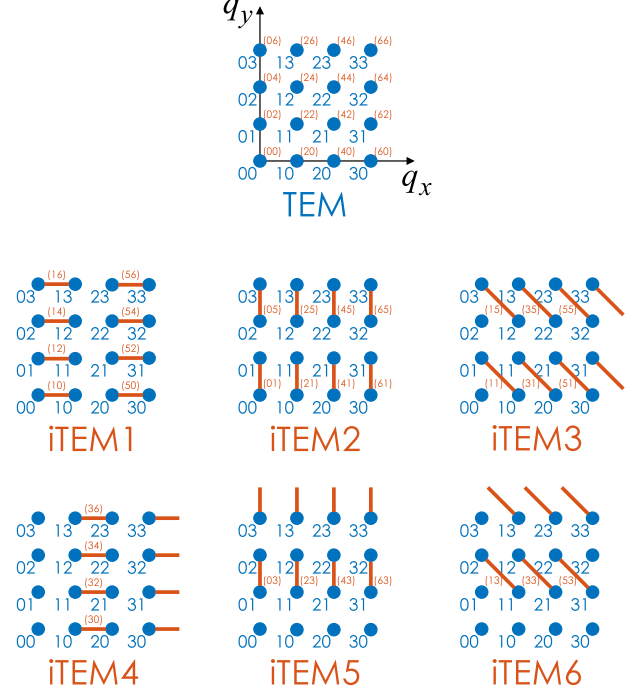


FIG. 1. Each dot corresponds to a TEM mode in the (q_x, q_y) space, and each line connecting two dots denotes an interferometer between two modes in an iTEM scheme. The bracketed numbers are the orders (μ_X, μ_Y) of the moment parameters to which the projections are sensitive. The unconnected dots in some of the iTEM schemes denote the rest of the modes in a complete basis, which can be measured simultaneously to provide extra information.

V. COMPARISON WITH DIRECT IMAGING

Although the proposed SPADE measurements can in principle perform general imaging, their complexity would not be justifiable if they did not offer any significant advantage over direct imaging. To analyze the performance of direct imaging with a Gaussian PSF, expand $|\psi(\mathbf{r} - \mathbf{R})|^2$ in a Taylor series to obtain

$$\lambda(\mathbf{r}|\theta') = |\phi_{00}(\mathbf{r})|^2 \left[1 + \sum_{\boldsymbol{\mu}} D_{\boldsymbol{\mu}}(\mathbf{r})\theta'_{\boldsymbol{\mu}} \right], \quad (5.1)$$

$$D_{\boldsymbol{\mu}}(\mathbf{r}) \equiv \frac{\text{He}_{\mu_X}(x) \text{He}_{\mu_Y}(y)}{\boldsymbol{\mu}!}, \quad (5.2)$$

$$\theta'_{\boldsymbol{\mu}} \equiv \int d^2\mathbf{R} \Lambda(\mathbf{R}|\theta') X^{\mu_X} Y^{\mu_Y}. \quad (5.3)$$

Scheme	Projections	Mode index q_x	Mode index q_y	Moment order μ_X	Moment order μ_Y
TEM	$ \mathbf{q}\rangle$	\mathbb{N}	\mathbb{N}	even	even
iTEM1	$[\mathbf{q}\rangle \pm \mathbf{q} + (1, 0)\rangle]/\sqrt{2}$	even	\mathbb{N}	1, 5, 9, ...	even
iTEM2	$[\mathbf{q}\rangle \pm \mathbf{q} + (0, 1)\rangle]/\sqrt{2}$	\mathbb{N}	even	even	1, 5, 9, ...
iTEM3	$[\mathbf{q}\rangle \pm \mathbf{q} + (1, -1)\rangle]/\sqrt{2}$	\mathbb{N}	odd	odd	1, 5, 9, ...
iTEM4	$[\mathbf{q}\rangle \pm \mathbf{q} + (1, 0)\rangle]/\sqrt{2}$	odd	\mathbb{N}	3, 7, 11, ...	even
iTEM5	$[\mathbf{q}\rangle \pm \mathbf{q} + (0, 1)\rangle]/\sqrt{2}$	\mathbb{N}	odd	even	3, 7, 11, ...
iTEM6	$[\mathbf{q}\rangle \pm \mathbf{q} + (1, -1)\rangle]/\sqrt{2}$	\mathbb{N}	even	odd	3, 7, 11, ...

TABLE I. A list of measurement schemes, their projections, and the moment parameters to which they are sensitive.

In terms of this parameterization, the information becomes

$$J_{\mu\nu}^{(\text{direct})}(\theta') = N \int d^2\mathbf{r} |\phi_{00}(\mathbf{r})|^2 \frac{D_{\mu}(\mathbf{r})D_{\nu}(\mathbf{r})}{1 + \sum_{\eta} D_{\eta}(\mathbf{r})\theta'_{\eta}}. \quad (5.4)$$

Assume now that the support of the source distribution is centered at the origin and has a maximum width Δ much smaller than the PSF width, viz.,

$$\Delta \ll 1, \quad (5.5)$$

which defines the subdiffraction regime. The parameters are then bounded by

$$|\theta'_{\mu}| \leq \left(\frac{\Delta}{2}\right)^{|\mu|_1}, \quad (5.6)$$

and the image is so blurred that it resembles the TEM_{00} mode rather than the object, viz.,

$$\lambda(\mathbf{r}|\theta') = |\phi_{00}(\mathbf{r})|^2 [1 + O(\Delta)]. \quad (5.7)$$

The Cramér-Rao bound becomes

$$\text{CRB}_{\mu\nu}^{(\text{direct})}(\theta') = \frac{\mu!}{N} [\delta_{\mu\nu} + O(\Delta)]. \quad (5.8)$$

This generalizes the earlier results on direct imaging of two sources [15–17] and sets a fundamental limit to the precision of direct imaging with data processing [23, 45].

The small-object assumption also means that the Gaussian in Eq. (4.7) can be neglected, and the θ_{μ} parameters defined there becomes $\theta'_{\mu} + O(\Delta^{|\mu|_1+2})$. Equation (5.8) can then be compared with the bound for SPADE. For even μ_X and μ_Y , the information must be at least the amount provided by the TEM measurement, so a precision enhancement factor can be defined in terms of Eq. (4.10) and given by

$$\frac{\text{CRB}_{\mu\mu}^{(\text{direct})}}{\text{CRB}_{\mu\mu}^{(\text{TEM})}} \approx \frac{N^{(\text{TEM})}}{N} \frac{\mu!}{2^{|\mu|_1} (\mu/2)! \theta_{\mu}}. \quad (5.9)$$

Apart from a factor $N^{(\text{TEM})}/N$ determined by the different photon numbers detectable in each method, the important point is that the factor scales inversely with $\theta_{\mu} \leq (\Delta/2)^{|\mu|_1}$, so the enhancement is enormous in the $\Delta \ll 1$ subdiffraction regime. The prefactor also increases with increasing μ .

For the other moments, the Cramér-Rao bound for SPADE must be lower than Eq. (4.14), which assumes an unknown β . An enhancement factor can be expressed as

$$\frac{\text{CRB}_{\mu\mu}^{(\text{direct})}}{\text{CRB}_{\mu\mu}^{(\mathbf{q}, \mu - \mathbf{q})}} \approx \frac{N^{(\text{iTEM})}}{N} \binom{\mu}{\mathbf{q}} \frac{1}{2^{2|\mu|_1-1} \beta(\mathbf{q}, \mu - \mathbf{q})}, \quad (5.10)$$

$$\binom{\mu}{\mathbf{q}} \equiv \frac{\mu!}{\mathbf{q}!(\mu - \mathbf{q})!}. \quad (5.11)$$

With $\beta(\mathbf{q}, \mu - \mathbf{q}) = O(\Delta^{\min[2q_{|1|}, |2(\mu - \mathbf{q})|_{|1|}]}),$ both $1/\beta$ and the coefficient defined by Eq. (5.11) can be maximized by choosing \mathbf{q} to be as close to $\mu/2$ as possible. This justifies the pairing of neighboring modes in the iTEM schemes listed in Table I and Fig. 1. With iTEM1, iTEM2, iTEM4, and iTEM5, $|\mu|_1$ is odd, and

$$\beta = O(\Delta^{|\mu|_1-1}). \quad (5.12)$$

With iTEM3 and iTEM6, $|\mu|_1$ is even, and

$$\beta = O(\Delta^{|\mu|_1}). \quad (5.13)$$

The enhancements can again be significant, except for the first moments θ_{10} and θ_{01} , which determine the object centroid and can be well estimated by direct imaging.

These results can be compared with Refs. [1, 2] for the special case of two equally bright point sources. If the origin of the image plane is aligned with their centroid and their separation along the X direction is d , $\theta_{20} \approx \theta'_{20} = d^2/4$, and a reparameterization leads to $\mathcal{J}^{(\text{direct})}(d) \approx Nd^2/8$ and $\mathcal{J}^{(\text{TEM})}(d) \approx N/4$ with respect to d , in accordance with the results in Refs. [1, 2] to the leading order of d . The experiments reported in Refs. [11–13] serve as demonstrations of the proposed scheme in this special case.

VI. NUMERICAL DEMONSTRATION

Here I present a numerical study to illustrate the proposal and confirm the theory. Assume an object that consists of 5 equally bright point sources with random positions within the square $-0.3 \leq X \leq 0.3$ and $-0.3 \leq Y \leq 0.3$. The average photon number is assumed to be $N = 5 \times 10,000$ in total. Figure 2 shows an example of the generated source positions

and a direct image with pixel size $\delta x \delta y = 0.1 \times 0.1$ and Poisson noise. I focus on the estimation of the first and second moments of the source distribution, viz.,

$$\{\theta'_\mu; \mu = (1, 0), (0, 1), (2, 0), (0, 2), (1, 1)\}. \quad (6.1)$$

For direct imaging, I use the estimator

$$\check{\theta}'_\mu = \frac{\mu!}{N} \sum_j D_\mu(\mathbf{r}_j) m(\mathbf{r}_j), \quad (6.2)$$

where $m(\mathbf{r}_j)$ is the photon count at a pixel positioned at \mathbf{r}_j . It can be shown that, in the small-pixel limit, this estimator is unbiased and approaches the Cramér-Rao bound given by Eq. (5.8) for $\Delta \ll 1$.

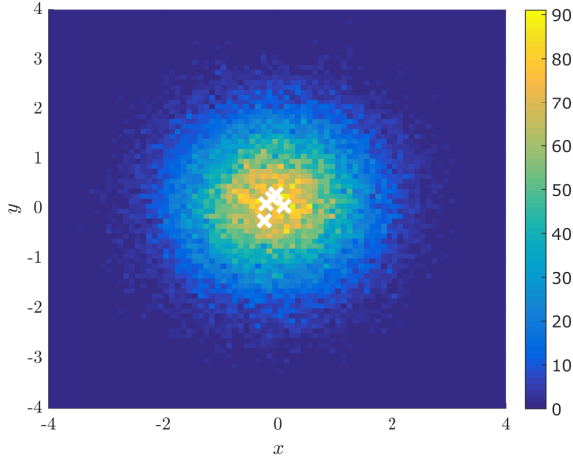


FIG. 2. The white crosses denote the 5 randomly generated source positions. The background image is a direct image with pixel size $dxdy = 0.1 \times 0.1$ (normalized with respect to the PSF width) and Poisson noise; the average photon number is $N = 5 \times 10,000$ in total.

For SPADE, I consider only the TEM₀₀, TEM₁₀, and TEM₀₁ modes, and the photons in all the other modes are discarded. As illustrated in Fig. 3, the iTEM1, iTEM2, and iTEM3 schemes suffice to estimate the parameters of interest. Table II lists the projections, and Fig. 4 plots the spatial wave functions for the projections. The light is assumed to be split equally among the three schemes, leading to 9 outputs; Fig. 5 shows a sample of the photon counts simulated with Poisson statistics. Compared with the large number of pixels in direct imaging, the compressive nature of SPADE for moment estimation is an additional advantage.

For the estimator, I ignore the difference between θ_μ and θ'_μ and assume

$$\begin{aligned} \check{\theta}'_{10} &= \frac{3}{N} (m_{11} - m_{21}), & \check{\theta}'_{01} &= \frac{3}{N} (m_{12} - m_{22}), \\ \check{\theta}'_{20} &= \frac{12}{N} m_{32}, & \check{\theta}'_{02} &= \frac{12}{N} m_{31}, \\ \check{\theta}'_{11} &= \frac{6}{N} (m_{13} - m_{23}), \end{aligned} \quad (6.3)$$

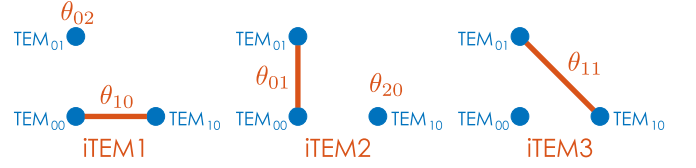


FIG. 3. A graphical representation of the iTEM1, iTEM2, and iTEM3 schemes involving the three TEM modes to be measured. Each line denotes an interferometer between two modes, and each unconnected dot denotes a TEM mode to be measured. The modes are also denoted by the parameters θ_μ to which they are sensitive.

iTEM1	iTEM2	iTEM3
$(00\rangle + 10\rangle)/\sqrt{2}$	$(00\rangle + 01\rangle)/\sqrt{2}$	$(10\rangle + 01\rangle)/\sqrt{2}$
$(00\rangle - 10\rangle)/\sqrt{2}$	$(00\rangle - 01\rangle)/\sqrt{2}$	$(10\rangle - 01\rangle)/\sqrt{2}$
$ 01\rangle$	$ 10\rangle$	$ 00\rangle$

TABLE II. The projections for the SPADE measurement scheme depicted in Fig. 3. $|00\rangle$ corresponds to the TEM₀₀ mode, $|10\rangle$ corresponds to the TEM₁₀ mode, and $|01\rangle$ corresponds to the TEM₀₁ mode.

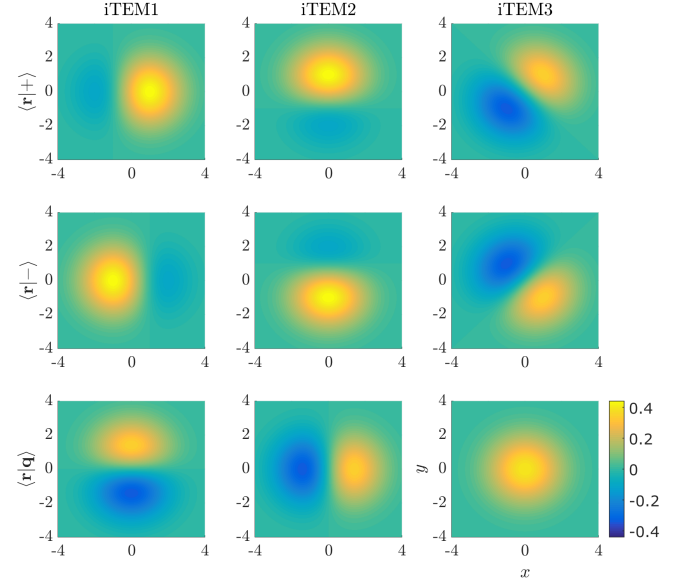


FIG. 4. The spatial wave functions $\langle \mathbf{r} | \phi_j \rangle$ for the projections listed in Table II. x and y are image-plane coordinates normalized with respect to the PSF width and the color code corresponds to amplitudes of normalized wave functions.

where m_{jk} are the photon counts of the 9 outputs, following the order in Table II and Figs. 4 and 5. This estimator is unbiased and comes from a straightforward inversion of Eqs. (4.9) and (4.12), assuming an average of $N/3$ photons available to each scheme. The iTEM backgrounds contain more information about θ'_{20} and θ'_{02} that can be used in a more complicated estimator to lower the errors further, but the simple estimator here suffices for the demonstration.

Figure 6 plots the numerically computed mean-square errors (MSEs) for 100 randomly generated objects versus true

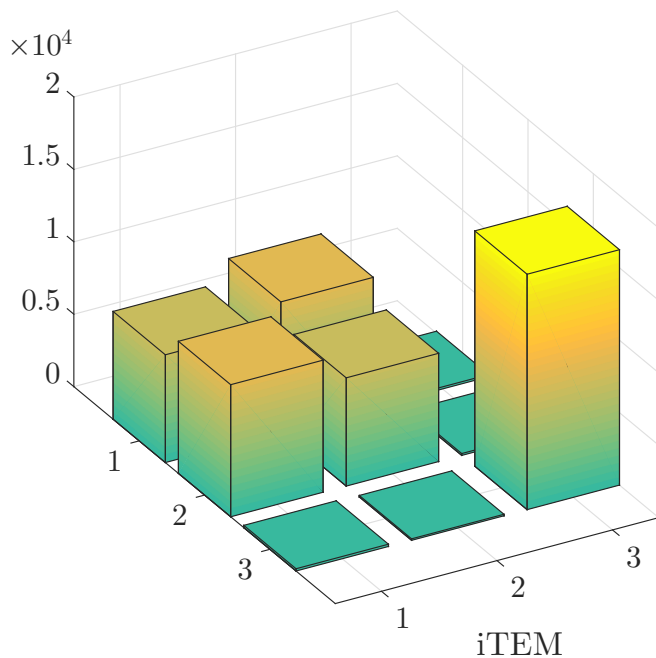


FIG. 5. A sample of the simulated photon counts from SPADE. The order of the matrix elements follows Table II and Fig. 4.

parameters in log-log scale. Each error value for a given object is computed by averaging the squared difference between the estimator and the true parameter over 500 samples of Poissonian outputs. For comparison, Fig. 6 also plots the Cramér-Rao bounds given by Eqs. (4.10), (4.14), and (5.8), assuming $\theta_\mu = \theta'_\mu$ and neglecting the $O(\Delta)$ term in Eq. (5.8). A few observations can be made:

1. As shown by the plots in the first row of Fig. 6, SPADE is 3 times worse than direct imaging at estimating the first moments. This is because SPADE uses only 1/3 of the available photons to estimate each first moment.
2. The other plots show that SPADE is substantially more precise at estimating the second moments, even though SPADE uses only a fraction of the available photons to estimate each moment. This enhancement is a generalization of the recent results on two sources [1–6, 8–13].
3. The errors are all remarkably tight to the Cramér-Rao bounds, despite the simplicity of the estimators and the approximations in deriving the bounds.

VII. DISCUSSION

Intuitively, the enhancements offered by SPADE can be understood by inspecting the form of the Fisher information given by Eq. (3.4). Consider the single-parameter information for a given θ_μ . The linear parameterization used here means that the mean intensity of each output, $\propto p(j|\theta)$, consists of a signal component $\propto \theta_\mu$ and a θ_μ -independent background.

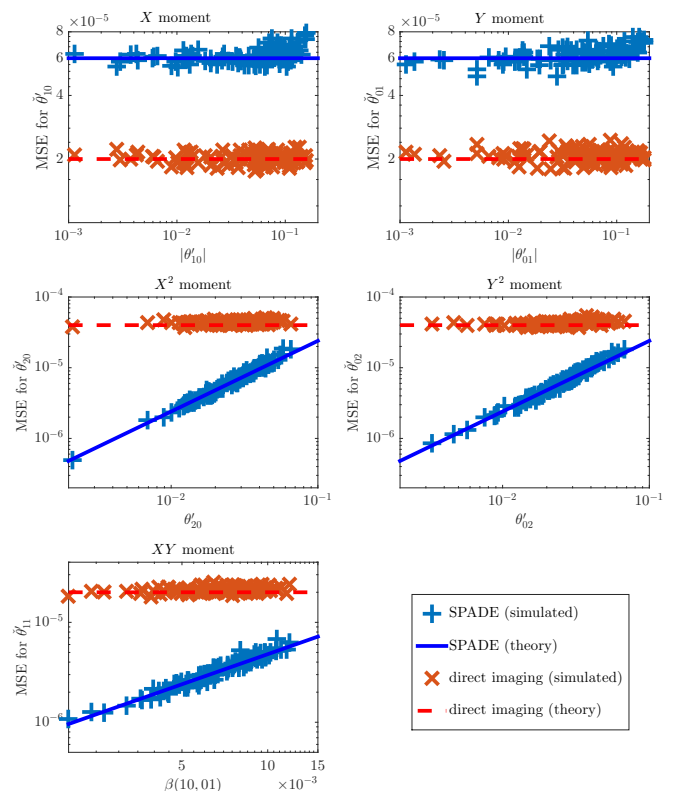


FIG. 6. Simulated errors for SPADE and direct imaging versus certain parameters of interest in log-log scale. The lines are the Cramér-Rao bounds given by Eqs. (4.10), (4.14), and (5.8), assuming $\theta_\mu = \theta'_\mu$ and neglecting the $O(\Delta)$ term in Eq. (5.8). Recall that all lengths are normalized with respect to the PSF width σ , so the first moments θ'_{10} and θ'_{01} are in units of σ , their MSEs are in units of σ^2 , the second moments θ'_{20} , θ'_{02} , θ'_{11} , and $\beta(10, 01) = (\theta'_{20} + \theta'_{02})/8$ are in units of σ^2 , and their MSEs are in units of σ^4 .

To maximize the information, the background should be minimized to reduce the denominator in Eq. (3.4). In other words, with shot noise, it is desirable to have dark ports, as is well known in optical interferometry. In the subdiffraction regime, the TEM₀₀ mode dominates the background in direct imaging, as indicated by Eq. (5.1). SPADE, on the other hand, is able to lower the background for each output by filtering out irrelevant low-order TEM modes. To wit, Eq. (4.9) for TEM measurements has zero background, while Eqs. (4.12) for iTEM also have low backgrounds in the subdiffraction regime. In this respect, the proposed scheme seems to work in a similar way to nulling interferometry for exoplanet detection [46, 47]. The nulling was used there for the special purpose of blocking the emission of a star, however, and there had not been any prior statistical study of nulling in the subdiffraction regime to my knowledge. The surprise here is that such coherent optical processing in the far field can vastly improve subdiffraction incoherent imaging, without the need to manipulate the sources like prior superresolution microscopic methods [48–51].

To be sure, the giant enhancements do not imply unlimited resolution for finite photon numbers. The reconstruc-

tion of the full source distribution from either low-frequency data or finite moments is ill posed [52], unless prior information is available to justify regularization [52–55]. Even if the moments are of primary interest, the higher moments are still more difficult to estimate with SPADE, as the fractional error $\sim \text{CRB}_{\mu\mu}/\theta_\mu^2$ is $1/O(N\Delta^{|\mu|_1})$ for even $|\mu|_1$ and $1/O(N\Delta^{|\mu|_1+1})$ for odd $|\mu|_1$, meaning that more photons are needed to achieve a satisfactory fractional error for higher $|\mu|_1$. Provided that enough photons can be collected, however, the enhanced precision in moment estimation should still be useful for many imaging applications [24]. For example, the size and shape of a star, a planetary system, or a fluorescent cluster that is poorly resolved under direct imaging can be identified much more accurately through the estimation of higher moments by SPADE. In view of the results in Refs. [2–4], the interferometric schemes proposed in Refs. [2–4, 19–22] are expected to be similarly useful for estimating the second moments at least. For larger objects, scanning in the manner of confocal microscopy [25] should be useful.

Many open problems remain; chief among them are the incorporation of prior information, generalizations for non-Gaussian PSFs, the derivation of fundamental quantum limits, and optimal experimental design. These are daunting problems, but may be attacked by more advanced methods in quantum metrology [56–61], quantum state tomography [62–65], and compressed sensing [53–55, 64, 65].

ACKNOWLEDGMENTS

Inspiring discussions with Ranjith Nair, Xiao-Ming Lu, Shan Zheng Ang, Shilin Ng, Laura Waller’s group, Geoff Stiebing, and Ben Recht are gratefully acknowledged. This work is supported by the Singapore National Research Foundation under NRF Grant No. NRF-NRFF2011-07 and the Singapore Ministry of Education Academic Research Fund Tier 1 Project R-263-000-C06-112.

-
- [1] Mankei Tsang, Ranjith Nair, and Xiao-Ming Lu, “Quantum theory of superresolution for two incoherent optical point sources,” *Physical Review X* **6**, 031033 (2016).
- [2] Shan Zheng Ang, Ranjith Nair, and Mankei Tsang, “Quantum limit for two-dimensional resolution of two incoherent optical point sources,” [arXiv:1606.00603 \[physics, physics:quant-ph\]](https://arxiv.org/abs/1606.00603) (2016), arXiv: 1606.00603.
- [3] Ranjith Nair and Mankei Tsang, “Interferometric superlocalization of two incoherent optical point sources,” *Opt. Express* **24**, 3684–3701 (2016).
- [4] Ranjith Nair and Mankei Tsang, “Far-Field Superresolution of Thermal Electromagnetic Sources at the Quantum Limit,” *Physical Review Letters* **117**, 190801 (2016).
- [5] Mankei Tsang, Ranjith Nair, and Xiao-Ming Lu, “Quantum information for semiclassical optics,” in *Proc. SPIE, Quantum and Nonlinear Optics IV*, Vol. 10029 (2016) pp. 1002903–1002903–7.
- [6] Mankei Tsang, “Conservative error measures for classical and quantum metrology,” [arXiv:1605.03799 \[physics, physics:quant-ph\]](https://arxiv.org/abs/1605.03799) (2016), arXiv: 1605.03799.
- [7] Xiao-Ming Lu, Ranjith Nair, and Mankei Tsang, “Quantum-optimal detection of one-versus-two incoherent sources with arbitrary separation,” [arXiv:1609.03025 \[quant-ph\]](https://arxiv.org/abs/1609.03025) (2016), arXiv: 1609.03025.
- [8] Cosmo Lupo and Stefano Pirandola, “Ultimate Precision Bound of Quantum and Subwavelength Imaging,” *Physical Review Letters* **117**, 190802 (2016).
- [9] J. Rehacek, M. Paur, B. Stoklasa, L. Motka, Z. Hradil, and L. L. Sanchez-Soto, “Dispelling Rayleigh’s Curse,” [arXiv:1607.05837 \[quant-ph\]](https://arxiv.org/abs/1607.05837) (2016), arXiv: 1607.05837.
- [10] Zong Sheng Tang, Kadir Durak, and Alexander Ling, “Fault-tolerant and finite-error localization for point emitters within the diffraction limit,” *Optics Express* **24**, 22004 (2016).
- [11] Fan Yang, Arina Tashchilina, E. S. Moiseev, Christoph Simon, and A. I. Lvovsky, “Far-field linear optical superresolution via heterodyne detection in a higher-order local oscillator mode,” *Optica* **3**, 1148 (2016).
- [12] Weng Kian Tham, Hugo Ferretti, and Aephraim M. Steinberg, “Beating Rayleigh’s Curse by Imaging Using Phase Information,” [arXiv:1606.02666 \[physics, physics:quant-ph\]](https://arxiv.org/abs/1606.02666) (2016), arXiv: 1606.02666.
- [13] Martin Pař, Bohumil Stoklasa, Zdenek Hradil, Luis L. Sánchez-Soto, and Jaroslav Rehacek, “Achieving the ultimate optical resolution,” *Optica* **3**, 1144 (2016).
- [14] Hari Krovi, Saikat Guha, and Jeffrey H. Shapiro, “Attaining the quantum limit of passive imaging,” [arXiv:1609.00684 \[physics, physics:quant-ph\]](https://arxiv.org/abs/1609.00684) (2016), arXiv: 1609.00684.
- [15] E. Bettens, D. Van Dyck, A. J. den Dekker, J. Sijbers, and A. van den Bos, “Model-based two-object resolution from observations having counting statistics,” *Ultramicroscopy* **77**, 37–48 (1999).
- [16] S. Van Aert, A. J. den Dekker, D. Van Dyck, and A. van den Bos, “High-resolution electron microscopy and electron tomography: resolution versus precision,” *Journal of Structural Biology* **138**, 21–33 (2002).
- [17] Sripad Ram, E. Sally Ward, and Raimund J. Ober, “Beyond Rayleigh’s criterion: A resolution measure with application to single-molecule microscopy,” *Proceedings of the National Academy of Sciences of the United States of America* **103**, 4457–4462 (2006).
- [18] Carmen O. Acuna and Joseph Horowitz, “A statistical approach to the resolution of point sources,” *Journal of Applied Statistics* **24**, 421–436 (1997).
- [19] Nicolas Sandeau and Hugues Giovannini, “Increasing the lateral resolution of 4pi fluorescence microscopes,” *Journal of the Optical Society of America A* **23**, 1089 (2006).
- [20] Kai Wicker and Rainer Heintzmann, “Interferometric resolution improvement for confocal microscopes,” *Optics Express* **15**, 12206 (2007).
- [21] Kai Wicker, Simon Sindbert, and Rainer Heintzmann, “Characterisation of a resolution enhancing image inversion interferometer,” *Optics Express* **17**, 15491 (2009).
- [22] D. Weigel, R. Foerster, H. Babovsky, A. Kiessling, and R. Kowarschik, “Enhanced resolution of microscopic objects by image inversion interferometry,” *Optics Express* **19**, 26451 (2011).
- [23] David J. Brady, *Optical Imaging and Spectroscopy* (Wiley, Hoboken, 2009).

- [24] Richard J. Prokop and Anthony P. Reeves, "A survey of moment-based techniques for unoccluded object representation and recognition," *CVGIP: Graphical Models and Image Processing* **54**, 438–460 (1992).
- [25] James B. Pawley, ed., *Handbook of Biological Confocal Microscopy* (Springer, New York, 2006).
- [26] Hendrik Deschout, Francesca Cella Zanacchi, Michael Mlodzianoski, Alberto Diaspro, Joerg Bewersdorf, Samuel T. Hess, and Kevin Braeckmans, "Precisely and accurately localizing single emitters in fluorescence microscopy," *Nature Methods* **11**, 253–266 (2014).
- [27] Kim I. Mortensen, L. Stirling Churchman, James A. Spudich, and Henrik Flyvbjerg, "Optimized localization analysis for single-molecule tracking and super-resolution microscopy," *Nature Methods* **7**, 377–381 (2010).
- [28] Jerry Chao, E. Sally Ward, and Raimund J. Ober, "Fisher information theory for parameter estimation in single molecule microscopy: tutorial," *Journal of the Optical Society of America A* **33**, B36 (2016).
- [29] Jonas Zmuidzinas, "Cramér–Rao sensitivity limits for astronomical instruments: implications for interferometer design," *J. Opt. Soc. Am. A* **20**, 218–233 (2003).
- [30] Martin C. E. Huber, Anuschka Pauluhn, J. Len Culhane, J. Gethyn Timothy, Klaus Wilhelm, and Alex Zehnder, eds., *Observing Photons in Space: A Guide to Experimental Space Astronomy* (Springer, New York, 2013).
- [31] Joseph W. Goodman, *Statistical Optics* (Wiley, New York, 1985).
- [32] Jeffrey H. Shapiro, "The quantum theory of optical communications," *IEEE Journal of Selected Topics in Quantum Electronics* **15**, 1547–1569 (2009).
- [33] Joseph W. Goodman, *Introduction to Fourier Optics* (McGraw-Hill, New York, 2004).
- [34] Larry A. Wasserman, *All of Statistics* (Springer, New York, 2004).
- [35] Carl W. Helstrom, "Resolvability of objects from the standpoint of statistical parameter estimation," *J. Opt. Soc. Am.* **60**, 659–666 (1970).
- [36] L. Motka, B. Stoklasa, M. D'Angelo, P. Facchi, A. Garuccio, Z. Hradil, S. Pascazio, F. V. Pepe, Y. S. Teo, J. Řeháček, and L. L. Sánchez-Soto, "Optical resolution from Fisher information," *The European Physical Journal Plus* **131**, 130 (2016).
- [37] Ram Zamir, "A proof of the Fisher information inequality via a data processing argument," *IEEE Transactions on Information Theory* **44**, 1246–1250 (1998).
- [38] Amnon Yariv, *Quantum Electronics* (Wiley, New York, 1989).
- [39] DLMF, "NIST Digital Library of Mathematical Functions," <http://dlmf.nist.gov/>, Release 1.0.11 of 2016-06-08, online companion to [40].
- [40] Frank W. J. Olver, Daniel W. Lozier, Ronald F. Boisvert, and Charles W. Clark, eds., *NIST Handbook of Mathematical Functions* (Cambridge University Press, New York, NY, 2010) print companion to [39].
- [41] Leonard Mandel and Emil Wolf, *Optical Coherence and Quantum Optics* (Cambridge University Press, Cambridge, 1995).
- [42] Jean-François Morizur, Lachlan Nicholls, Pu Jian, Seiji Armstrong, Nicolas Treps, Boris Hage, Magnus Hsu, Warwick Bowen, Jiri Janousek, and Hans-A. Bachor, "Programmable unitary spatial mode manipulation," *J. Opt. Soc. Am. A* **27**, 2524–2531 (2010).
- [43] Seiji Armstrong, Jean-François Morizur, Jiri Janousek, Boris Hage, Nicolas Treps, Ping Koy Lam, and Hans-A. Bachor, "Programmable multimode quantum networks," *Nature Commun.* **3**, 1026 (2012).
- [44] Kevin Piché, Jonathan Leach, Allan S. Johnson, Jeff Z. Salvail, Mikhail I. Kolobov, and Robert W. Boyd, "Experimental realization of optical eigenmode super-resolution," *Opt. Express* **20**, 26424–26433 (2012).
- [45] Mario Bertero and Christine de Mol, "III Super-Resolution by Data Inversion," in *Progress in Optics*, Vol. 36, edited by E. Wolf (Elsevier, Amsterdam, 1996) pp. 129–178.
- [46] R. N. Bracewell, "Detecting nonsolar planets by spinning infrared interferometer," *Nature* **274**, 780–781 (1978).
- [47] M. A. C. Perryman, "Extra-solar planets," *Reports on Progress in Physics* **63**, 1209 (2000).
- [48] William E. Moerner, "New directions in single-molecule imaging and analysis," *Proceedings of the National Academy of Sciences* **104**, 12596–12602 (2007).
- [49] Eric Betzig, George H. Patterson, Rachid Sougrat, O. Wolf Lindwasser, Scott Olenych, Juan S. Bonifacino, Michael W. Davidson, Jennifer Lippincott-Schwartz, and Harald F. Hess, "Imaging intracellular fluorescent proteins at nanometer resolution," *Science* **313**, 1642–1645 (2006).
- [50] Stefan W. Hell, "Far-field optical nanoscopy," *Science* **316**, 1153–1158 (2007).
- [51] Mikhail I. Kolobov, ed., *Quantum Imaging* (Springer, New York, 2007).
- [52] M. Bertero, "Linear Inverse and III-Posed Problems," in *Advances in Electronics and Electron Physics*, Vol. 75, edited by Peter W. Hawkes (Academic Press, 1989) pp. 1–120.
- [53] Yohann de Castro and Fabrice Gamboa, "Exact reconstruction using Beurling minimal extrapolation," *Journal of Mathematical Analysis and Applications* **395**, 336–354 (2012).
- [54] Emmanuel J. Candès and Carlos Fernandez-Granda, "Towards a Mathematical Theory of Super-resolution," *Communications on Pure and Applied Mathematics* **67**, 906–956 (2014).
- [55] Geoffrey Schiebinger, Elina Robeva, and Benjamin Recht, "Superresolution without Separation," ArXiv e-prints (2015), [arXiv:1506.03144 \[math.OC\]](https://arxiv.org/abs/1506.03144).
- [56] Carl W. Helstrom, *Quantum Detection and Estimation Theory* (Academic Press, New York, 1976).
- [57] Alexander S. Holevo, *Probabilistic and Statistical Aspects of Quantum Theory* (Edizioni della Normale, Pisa, Italy, 2011).
- [58] Masahito Hayashi, ed., *Asymptotic Theory of Quantum Statistical Inference: Selected Papers* (World Scientific, Singapore, 2005).
- [59] Jonas Kahn and Mădălin Guță, "Local Asymptotic Normality for Finite Dimensional Quantum Systems," *Communications in Mathematical Physics* **289**, 597–652 (2009).
- [60] Dominic W. Berry, Mankei Tsang, Michael J. W. Hall, and Howard M. Wiseman, "Quantum Bell-Ziv-Zakai Bounds and Heisenberg Limits for Waveform Estimation," *Phys. Rev. X* **5**, 031018 (2015).
- [61] Xiao-Ming Lu and Mankei Tsang, "Quantum Weiss-Weinstein bounds for quantum metrology," *Quantum Science and Technology* **1**, 015002 (2016).
- [62] Miroslav Jeek and Zdenk Hradil, "Reconstruction of spatial, phase, and coherence properties of light," *Journal of the Optical Society of America A* **21**, 1407 (2004).
- [63] A. I. Lvovsky and M. G. Raymer, "Continuous-variable optical quantum-state tomography," *Reviews of Modern Physics* **81**, 299–332 (2009).
- [64] David Gross, Yi-Kai Liu, Steven T. Flammia, Stephen Becker, and Jens Eisert, "Quantum state tomography via compressed sensing," *Phys. Rev. Lett.* **105**, 150401 (2010).
- [65] Jeongwan Haah, Aram W. Harrow, Zhengfeng Ji, Xiaodi Wu, and Nengkun Yu, "Sample-optimal tomography of quantum states," ArXiv e-prints (2015), [arXiv:1508.01797 \[quant-ph\]](https://arxiv.org/abs/1508.01797).